Confined diffusion of hydrophilic probes inserted in lyotropic lamellar phases

Patrick Moreau, Damien van Effenterre, Laurence Navailles, Frédéric Nallet, Didier Roux

Confined diffusion of hydrophilic probes inserted in lyotropic lamellar phases

P. Moreau, D. van Effenterre, L. Navailles*, F. Nallet and D. Roux†
Université Bordeaux-1
CNRS, Centre de recherche Paul-Pascal
115 avenue du Docteur-Schweitzer
F-33600 Pessac, France

February 27, 2008

Abstract

The dynamic behaviour of three hydrophilic probes (two dyes and one fluorescently-labelled protein) inserted in the water layers of lyotropic lamellar phases has been studied by confocal fluorescence recovery experiments. Two different, ionic (AOT/NaCl/H_2O) and non-ionic ($C_{12}E_5$/hexanol/H_2O) host systems were studied. The confinement effect has been carefully monitored using the swelling properties of the lamellar phases. In all cases, we measure the evolution of the probe diffusion coefficient in the layer plane $D_\perp$ *versus* the separation between the membranes d_w. Depending on the composition of the lamellar phase, this distance can be continuously adjusted from 500 Å to about 20 Å. For all systems, we observe a first regime, called dilute regime, where the diffusion coefficient decreases almost linearly with $1/d_w$. In this regime, the Faxén theory for the friction coefficient of a spherical particle symmetrically dragged between two rigid walls can largely explain our results. More unexpectedly, when the membranes are non ionic, and also quite flexible ($C_{12}E_5$/hexanol in water), we observe the existence of a second, concentrated (or confined) regime, where the diffusion coefficient is nearly constant and different from zero for membrane separations smaller than the particle size. This new regime can be heuristically explained by simple arguments taking into account the membrane fluidity.

PACS. 82.70.-y Disperse systems; complex fluids – 87.16.Dg Membranes, bilayers, and vesicles – 87.64.Tt Confocal microscopy – 82.56.Lz Diffusion

1 Introduction

Self-assembled fluids such as oil-water-surfactant mixtures have attracted considerable interest over the past two decades [1]. These systems can generate mesoscopic fluctuating surfaces such as membranes, leading to interesting static and dynamic properties. Among the large variety of structures observed, the lamellar phase is of fundamental interest. In this phase, membranes are piled up to form a regular smectic structure, constituting a unique model system to study membrane properties. It is then not surprising that many studies have been devoted to the experimental characterisation of these lamellar phases [2].

Since the pioneering investigations by Kékicheff *et al.* [3], there has been in recent years a growing interest in surfactant-based lamellar systems mixed with polymers [4–8] and colloidal

*Offprint requests to: navailles@crpp-bordeaux.cnrs.fr
†Current address: Saint-Gobain – Les Miroirs, 18 avenue d'Alsace, F-92096 La Défense CEDEX, France

particles [9,10]. The influence of nanometre-size inclusions on self-assembled amphiphilic systems is quite complex. For instance, inclusions can stabilise vesicles or liposomes, or destabilise a lamellar phase, leading to vesicles. A considerable amount of work deals with the insertion of biological molecules (DNA, proteins) in lipid host phases [11], having as a main goal drug delivery [12] or protein crystallisation [13, 14]. The insertion of synthetic nanoparticles with specific catalytic, optical or magnetic properties within compartmentalised host phases (formed by copolymers, polyelectrolytes or surfactants) is also a very active field.

Although the first investigations concerning confined Brownian motion in lyotropic phases were performed a long time ago [15,16], some aspects of this problem remain a subject of discussions [17–19]. The importance of understanding the motion of spheres or anisotropic particles in confined geometries lies in its applicability to the description of particles migrating in porous media or near fluid-solid or fluid-fluid boundaries [20], membranes [21,22], and cells interacting with surfaces [23].

In this paper, we focus on the experimental study of the dynamic properties of oriented, doped lamellar phases and we will in particular show the effect of the confinement on the evolution of the probe diffusion coefficient when changing the lamellar periodicity. The confinement we are referring to originates from the finite height of the *solvent* layers and does not occur, except in some limiting cases, *within* the surfactant membranes. Such a confinement is easily varied using the swelling properties of the lamellar phase by changing the amount of solvent (water): The distance between adjacent membranes can thus be continuously adjusted.

The formulation and characterisation of our experimental systems are specified in Section 2.1 and we detail in the following Section 2.2 the general method for analysing fluorescence recovery after photo bleaching (FRAP) experiments. Section 3 presents the results obtained using FRAP. We emphasise in particular the evolution of the diffusion coefficient with increasing confinement. In the last part, Section 4, we propose simple heuristic arguments accounting for the role of membrane fluidity on the mobility of a particle confined between two fluid walls.

2 Materials and methods

2.1 Formulation and characterisation of the systems

Three different probes were inserted inside two distinct lamellar phases. The fluorescently-labelled protein (rhodamin-conjugated Bovine Serum Albumin protein: BSA*) was purchased from Sigma and used without further purification. The hydrodynamic radius R_H of the BSA monomers is known to be close to 40 Å at room temperature [24]. The other two dyes, fluorescein ($\lambda_{\rm exc} = 4940$ Å and $\lambda_{\rm em} = 5200$ Å) and rhodamin ($\lambda_{\rm exc} = 5410$ Å and $\lambda_{\rm em} = 5720$ Å)–purchased from Aldrich and Invitrogen-Molecular Probes respectively–were also used as received. Their hydrodynamic radii have both been found close to 10 Å.

The first lamellar system was made with the well-known non-ionic n-pentaethyleneglycol monododecylether surfactant $C_{12}E_5$ (from Nikko Ltd), hexanol and water [25,26]. The bilayers in this system have a rather small bending elasticity at room temperature ($\kappa = 0.8 k_B T$) [26] and the lamellar structure is known to be stabilised by the Helfrich mechanism of steric repulsion ("undulation interaction") [27]. The repeat distance d of the smectic structure can vary continuously from 30 Å to more than 10^3 Å depending upon the membrane volume fraction.

The second lamellar system was made with the anionic surfactant sodium bis(2-ethylhexyl) sulfosuccinate (AOT), NaCl and water [28, 29]. Without added salt, the system is stabilised by electrostatic interactions. When salt is added (1 wt%) the long-range electrostatic interactions are screened and the lamellar phase is stabilised by the undulation interaction [29].

Even though the phase diagram with no added particle is well established in both cases [26,28, 29] when particles are added the phase limits may change. Elaborating the phase diagrams with inserted probes (protein or fluorescent dye) is a long but necessary process in order to identify unambiguously a homogeneous lamellar phase. For added BSA* (0.1 wt% in water, corresponding to 15 μM), we present in Fig. 1 two cuts of the phase diagram: One representing the phase boundaries in the salt concentration–surfactant volume fraction (ϕ_m) plane and the other one in

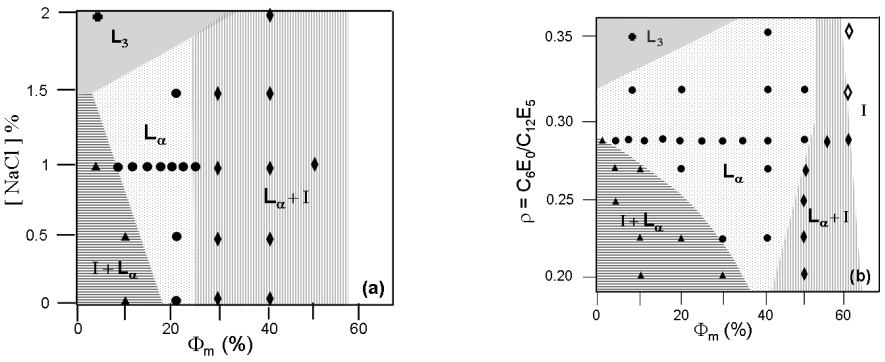

(a) (b)

Figure 1: Cuts of the phase diagram for systems doped with 15 μM of the fluorescent protein (BSA*) I: Isotropic phase, L_3: Sponge phase, L_α: Fluid lamellar phase. In (a), the cut of the phase diagram represents the phase boundaries in the salt concentration [NaCl] and surfactant volume fraction ϕ_m plane for the AOT / NaCl / water system. In (b), the cut of the phase diagram for the hexanol / $C_{12}E_5$ / water system represents the phase boundaries in the $\rho \equiv$ hexanol/$C_{12}E_5$ ratio and ϕ_m plane

the $\rho \equiv$ hexanol/$C_{12}E_5$ mass ratio–ϕ_m plane.

One-phase (isotropic: I, sponge phase: L_3 or lamellar phase: L_α) or two-phase (isotropic–lamellar, or micellar–lamellar domains) regions of the phase diagram have been characterised. The most important result is that the one-phase, BSA* doped lamellar phase is conserved for a large range of dilutions in both systems.

The systems formulated with and without doping particles have been characterised by polarising optical microscopy, fluorescence microscopy and x-ray scattering. X-ray scattering experiments were realised in order to describe the host phase nature (data not shown) and measure the lamellar spacing of L_α systems. We used polarising and fluorescence microscopy in order to confirm the localisation of the dye inside the lamellar phase. The optical observations were made using sealed flat capillaries of thickness 50 μm. As shown in Fig. 2, the typical texture of defects of the lamellar structure (oily streaks) appears. The fluorescence intensity is homogeneous in homeotropic domains.

Depending on the membrane volume fraction, these defects are more or less present and the

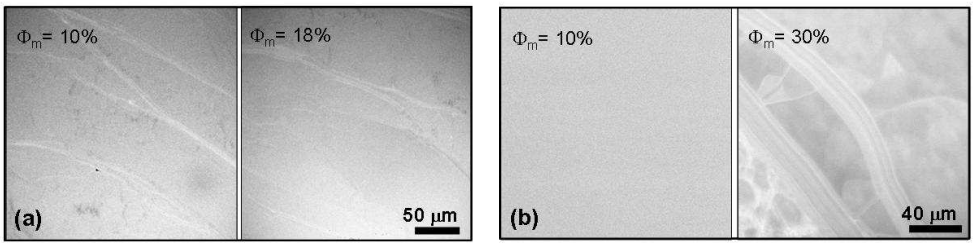

(a) (b)

Figure 2: Images obtained with the confocal fluorescent optical microscope. (a) AOT/NaCl/water/BSA* lamellar phase for two different membrane volume fractions ($\phi_m = 10\%$ and $\phi_m = 18\%$). (b) $C_{12}E_5$ / hexanol / water / BSA* lamellar phase for two different membrane volume fractions ($\phi_m = 10\%$ and $\phi_m = 30\%$)

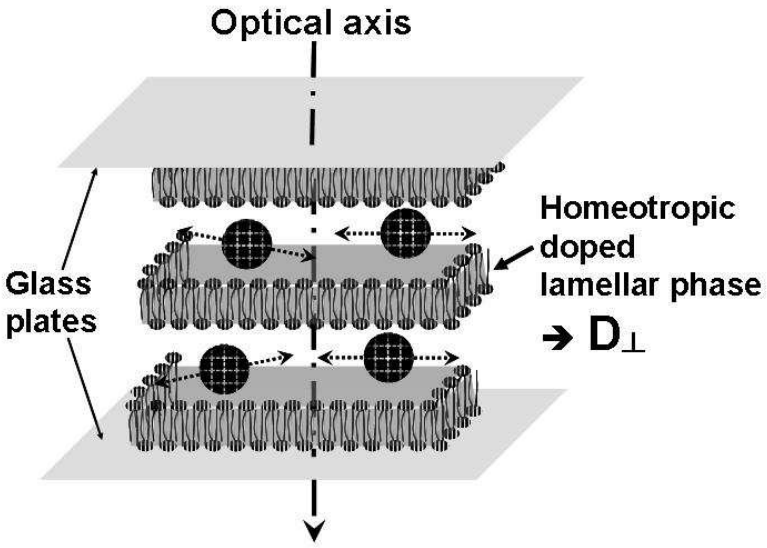

Figure 3: Schematic representation of the homeotropic orientation of the doped lamellar system inside a flat capillary. For FRAP experiments, the laser beam is parallel to the optical axis

orientation of the system can be disturbed. At high membrane concentrations, the dye can be expelled from the lamellar phase and the texture looses its homogeneity. In that case, the fluorescence intensity shows very bright fluorescent spots (aggregates) situated in the vicinity of the lamellar phase grain boundaries.

2.2 Diffusion coefficients: FRAP measurement

Within the last 30 years, fluorescence recovery after photo bleaching has become an important and versatile technique to study the dynamics in various systems [30], such as living cells, membranes and other biological environments. In polymer physics, the photo bleaching methods are employed to investigate diffusion in macromolecular systems, particularly in networks. The general principle of the FRAP technique [31] is to irreversibly photo bleach a certain region within a fluorescently labelled sample by irradiation with a short intense light pulse. Immediately after bleaching, a highly attenuated light beam is used to measure the recovery of fluorescence inside the bleached area as a result of the diffusion exchange of bleached fluorophores by unbleached molecules from the surroundings. Performing the experiment in a confocal laser scanning microscope (CLSM) gives high spatial resolution [32] and allows surgical bleaching.

In order to measure the translational diffusion coefficient parallel to the layers ($D_\perp$, *i.e.* perpendicular to the optical axis), we worked with homeotropically oriented lamellar phases. The flat capillary (thickness $e = 50$ μm) is filled by capillarity with the lamellar sample and is carefully sealed. The lamellar phase will naturally choose homeotropic anchoring (stacking axis perpendicular to the walls) and well oriented monodomains of millimetre sizes are obtained. The homeotropic orientation is checked using the optical polarising microscopy technique. As shown in Fig. 3, the laser beam is parallel to the normal of the layers.

The bleaching and imaging were performed on a Leica SP2 confocal microscope with an oil immersion 63× objective lens (numerical aperture 1.4). We bleach a spot area about $R \approx 2$ μm in radius during a bleaching time τ (in the range 1 to 10 seconds, depending on the dye bleached). The image acquisition is made by scanning the field with a confocal photomultiplier (acquisition time in the order of a few seconds) after a time t has elapsed.

In a first approximation, the lateral width of the laser beam spot can be neglected. Then,

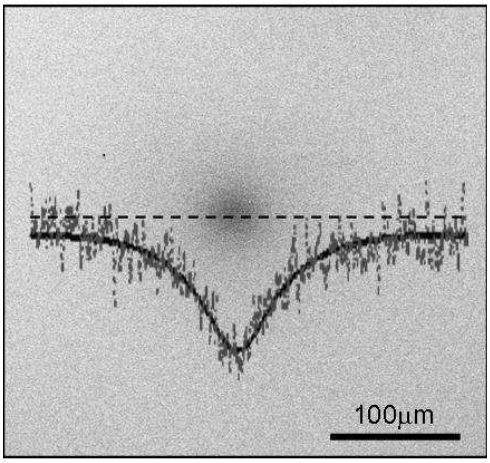

Figure 4: Example of an image obtained after bleaching (dark zone in the centre). The black dots correspond to the fluorescence profile along the dashed line and the black line to the interpolation by eq. (3)

assuming permeation through the bilayers to be negligible, the concentration of bleached dyes $c(r,t)$ *versus* space and time, initially non-zero only within the point-like laser spot, is found by integrating Fick's law in the 2D-space perpendicular to the optical axis, which leads to:

$$c(r,t) = \frac{c_0}{4\pi D_\perp t} \exp\left[-\frac{r^2}{4D_\perp t}\right] \tag{1}$$

when the bleaching duration is extremely short. In eq. (1), r is the distance from the centre of the bleach point, t the time, $D_\perp$ the diffusion coefficient in the layer plane, and c_0 is a normalisation constant depending on dye concentration, power of the bleaching radiation, etc.

For the sake of simplicity, the depletion in fluorescence intensity at time t after a photo bleaching of finite duration τ is represented as the superimposition of time-translated expressions similar to eq. (1), namely:

$$I(r,t,\tau) = \int_0^\tau \frac{I_0}{t-\tau_1} \exp\left[-\frac{r^2}{4D_\perp(t-\tau_1)}\right] d\tau_1 \tag{2}$$

with, of course, $t > \tau$, and I_0 a normalising constant. Using this scheme, the fluorescence intensity can therefore be described by the equation:

$$I(r,t,\tau) = I_0 \left(\mathrm{E}_1\left[\frac{r^2}{4D_\perp t}\right] - \mathrm{E}_1\left[\frac{r^2}{4D_\perp(t-\tau)}\right]\right) \tag{3}$$

with E_1 the exponential integral function of order 1. The diffusion coefficient $D_\perp$ is deduced from the recorded images by a numerical fitting using eq. (3), with only two fitting parameters, namely I_0 as an arbitrary intensity scale and $\sigma^2 \equiv 4D_\perp t$, since the bleaching duration τ is known. Figure 4 gives an example of the image obtained after bleaching. The dots correspond to the fluorescence profile along the dashed line, and the black line to the interpolation by eq. (3).

We have checked the validity of our description in terms of a Brownian dynamics for the particles by measuring the parameter σ^2 as a function of time: The Gaussian broadening should be a simple linear function of the elapsed time t, which is indeed observed.

Figure 5 shows the evolution of σ^2 *versus* time for the BSA* protein inserted in the AOT (Fig. 5a) and $C_{12}E_5$ (Fig. 5b) systems, respectively. From the observed linear behaviour, unambiguous values for the diffusion coefficient can be deduced. Similar results have been obtained with the other two fluorophores (data not shown).

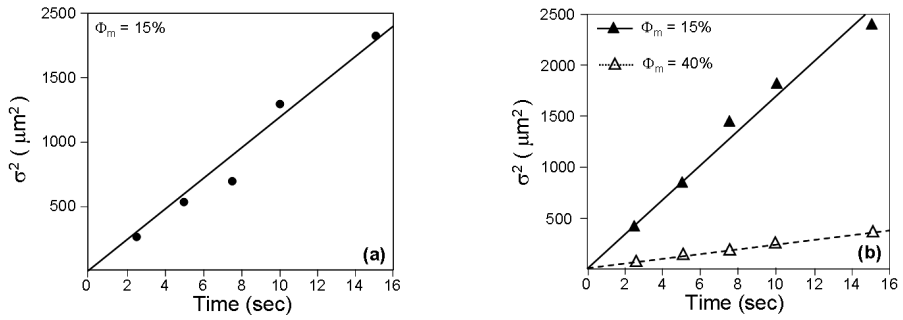

(a) (b)

Figure 5: Gaussian broadening σ^2 *versus* time t resulting from fits to eq. (3). The lines correspond to simple linear fits; (a) AOT / NaCl / water / BSA* system–membrane volume fraction $\phi_m = 15\%$; (b) $C_{12}E_5$ / hexanol / water / BSA* system for two different membrane volume fractions ($\phi_m = 15\%$ and $\phi_m = 40\%$)

Table 1: Free-diffusion coefficient D_0 and associated hydrodynamic radius R_H for the fluorescently-labelled protein (BSA*), the fluorescein and rhodamin dyes. For the hydrophobic probe (DHPE-FITC), the diffusion coefficient values refer to measurements in the lamellar phases, and R_H is computed from an estimate of the interfacial area of the DHPE lipid, see Section 4.5

	Fluorescein	Rhodamin	BSA*	DHPE-FITC	
D_0 $[10^{-12}\mathrm{m^2s^{-1}}]$	230 ± 22	193 ± 21	59 ± 3	$C_{12}E_5$: 7.9 ± 1	AOT: 18.3 ± 2.4
R_H [Å]	9 ± 1	11 ± 1	36 ± 3	4	

3 Results

We prepared samples with various water contents and, therefore, various water layer thicknesses (d_w). The quantity d_w is easily deduced from the swelling behaviour established with x-ray experiments: The stacking period d of the lamellar phase is first obtained from the value $q_{\max}$ of the first order Bragg peak as $d = 2\pi/q_{\max}$. Repeating the measurement for different concentrations, the bilayer thickness δ is extracted from the swelling law $d = \delta/\phi_m$. The water layer thickness is then easily deduced using the relation $d_w = d - \delta$. For systems without inserted particles, the swelling behaviour has been reported in previous studies [26, 29]. It turns out that the stacking periods are not appreciably modified after addition of either protein or probes. The membrane thickness δ is found to be equal to 28.7 Å, and 19.5 Å respectively, for the $C_{12}E_5$ and AOT systems.

Using FRAP experiments, we have measured for each probe the free-diffusion (D_0) coefficient in water (see Table 1). The experiment allows determining the associated hydrodynamic R_H radii with eq. (5), see below Section 4. As a reference for the confined limit, we also measured the diffusion coefficient of fluorescein 1,2-dihexadecanoyl-sn-glycero-3-phosphoethanolamine (DHPE-FITC, from Invitrogen – Molecular Probes), when this fluorescent, hydrophobic lipid is inserted into the membranes of homeotropically-oriented lamellar phases.

The effect of confinement is deduced from the measured self-diffusion coefficient $D_\perp$ of our probes or protein inserted in the lamellar phase. For each system, we plot–using semi-logarithmic scales–$D_\perp$ as a function of the water layer thickness d_w. The results obtained for the two probes (fluorescein and rhodamin) inside the $C_{12}E_5$ / hexanol / water lamellar phase are displayed in Fig. 6a. Figure 6b shows the results obtained for the protein (BSA*) in the two different lamellar systems ($C_{12}E_5$ and AOT).

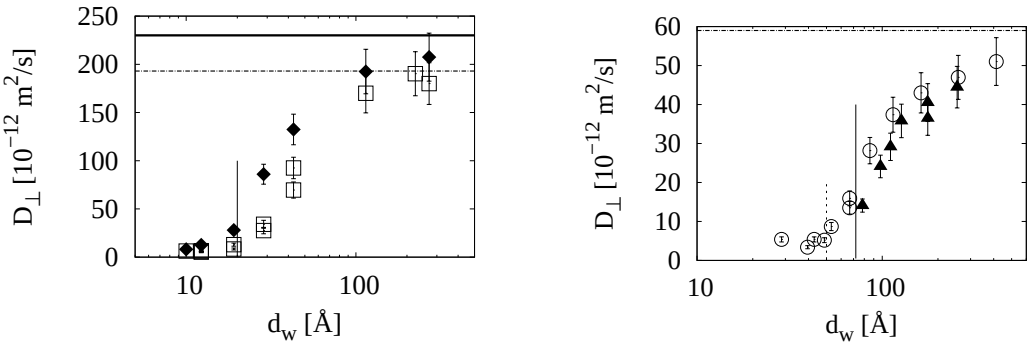

(a) (b)

Figure 6: Diffusion coefficient $D_\perp$ obtained from FRAP experiments *vs.* the water layer thickness d_w. The constant value of the free-diffusion coefficient is plotted as horizontal solid (fluorescein) or dash-dotted (rhodamin, BSA*) lines. (a) Fluorescein (filled lozenges ⧫) or rhodamin (empty squares □) dyes inserted in the lamellar phase of the $C_{12}E_5$ / hexanol / water system. Vertical solid line drawn at $d_w = 20$ Å. (b) Fluorescently-labelled protein (BSA*) inserted in the lamellar phase of the $C_{12}E_5$ / hexanol / water system (empty circle ∘) and of the AOT / NaCl / water system (filled triangles ▲). Vertical dotted (respectively, solid) line drawn at $d_w = 50$ Å (resp. $d_w = 72$ Å).

We observe (from large to small d_w) the following regimes: Values of $D_\perp$ close to the free-diffusion coefficient measured in bulk water are first obtained, then the diffusion coefficient significantly and steadily decreases, and third, a quasi-plateau where $D_\perp$ exhibits little or even no variations with d_w is reached. The fact that, at large d_w, the $D_\perp$ values asymptotically approach the diffusion coefficient for the probes in bulk water indicates that the probes do not interact with the surfactant. It appears in particular that, at contrast to what is sometimes observed with ionic surfactants [33], there is no significant unfolding of the protein. Moreover, the dyes do not adsorb onto the surfactant bilayers. If adsorption were an important effect, the diffusion coefficient would be mostly independent on swelling, as indeed observed for amphiphilic probes diffusing along the bilayers. As mentioned above, the diffusion coefficients of DHPE-FITC inserted into the same membranes have been measured. The values are very small and do not vary with the confinement, see data in Table 1.

The decrease of $D_\perp$ with decreasing d_w is due to the geometric confinement of the probe between the surfactant bilayers and will be more quantitatively interpreted later on. Interestingly, for very small membrane separations, we observe (except for the BSA*–AOT system, the protein being expelled from the lamellar phase) a regime where the diffusion coefficient does not go to negligible values at the point where the water layer thickness becomes equal to the particle diameter (vertical full lines in Fig. 6). The diffusion coefficient reaches a small, roughly constant value instead. This value is in the order of the diffusion coefficient for an amphiphilic dye inserted inside the same membrane. As mentioned above, this new (or confined) regime only appears for the $C_{12}E_5$ / hexanol / water system. It is also better defined in our experimental data with rhodamin or BSA* than with fluorescein. Though somehow arbitrarily defined, the boundary of the confined regime is not associated to a given value of d_w. For rhodamin, the transition may be considered to occur when the membrane separation becomes equal to the probe hydrodynamic diameter ($2R_H = 22$ Å). For BSA* at contrast, it is interesting to note that the transition apparently occurs for a d_w value (50 Å, vertical dotted line in Fig. 6b)) *smaller* than the hydrodynamic diameter of the protein (*ca.* 70 Å).

4 Discussion

As an explanation for the experimentally-observed transition between the dilute and confined regimes, associated with the fact that the diffusion coefficient does not reach a zero value when the confinement is equal to the particle size, "liquid" walls have to be considered. Theories available in the literature often describe confinement between *rigid* walls – [34–36], for instance– following the classical approach [37], the case of a particle near a fluid wall being considered, *e.g.*, in Ref. [20, 38].

Here, we shall not attempt to tackle the complete hydrodynamic problem, as it cannot be solved, in particular for particle and walls in near contact, without sophisticated and numerical methods [20]. We use heuristic arguments, instead. These non rigorous but simple arguments lead to representative limiting cases (including the confinement between rigid walls), as well as to an estimate the confinement between two *liquid* walls. The resulting description is found in good quantitative agreement with experimental data, see below Section 4.5.

4.1 3D diffusion

A hard sphere with radius R_H, moving with the constant velocity $\vec{v}_0$ in an unbound quiescent Newtonian fluid of viscosity η_0, experiences a hydrodynamic drag force $\vec{F}_0$ opposite to its direction of motion. This drag force is given in the small-velocity limit by the well-known Stokes law:

$$\vec{F}_0 = -6\pi\eta_0 R_H \vec{v}_0 \tag{4}$$

which defines the drag coefficient $\zeta \equiv 6\pi\eta_0 R_H$.

For sizes R_H in the colloidal range, the sphere is subject to Brownian motion. Classically, the self-diffusion coefficient D_0 of such a sphere suspended in a fluid at absolute temperature T is related to the drag coefficient as expressed in the Stokes-Einstein equation [39]:

$$D_0 = \frac{k_B T}{\zeta} = \frac{k_B T}{6\pi\eta_0 R_H} \tag{5}$$

where k_B is the Boltzmann constant.

4.2 Confined diffusion of a hard sphere

The experimental and theoretical study of the diffusion behaviour of a sphere close to a rigid wall, or confined between two parallel rigid walls, has been the object of an important number of works. Experimentally, the Brownian motion has been followed (in 3-dimensional geometries) both parallel to the walls [40–43], and perpendicular to them [42, 44–46] and also in quasi-2-dimensional geometries [47], this latter case allowing to work with anisotropic colloids [48].

On the theoretical side, even simple geometries lead to rather difficult problems. In one of its simplest–and oldest–version, the theoretical approach considers a rigid sphere moving near and parallel to a solid surface. In particular, Faxén [37] was able to express the drag coefficient for such a spherical particle located at an equal distance between two rigid walls. After conversion into a diffusion coefficient by means of the Stokes-Einstein relation, his expression reads, to lowest order:

$$D_\perp \approx D_0 \left[1 - 2\frac{R_H}{d_w}\right] \tag{6}$$

where D_0 is the value of the 3D diffusion coefficient of the particle, as given by eq. (5), R_H the hydrodynamics radius of the particle, and d_w the thickness of the fluid layer separating the two walls. Note that we keep naming axes, conventionally, with respect the optical axis of the lamellar phase: $D_\perp$ is actually associated to a motion *parallel* to the walls. Interestingly, eq. (6) results in $D_\perp \approx 0$ at the maximum possible confinement for sphere and walls that are both solid, namely $d_w \to 2R_H$. This limit appears physically to be quite natural, even though it is

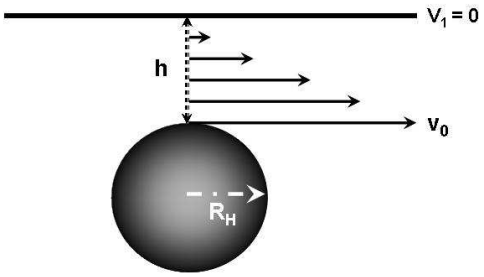

Figure 7: Schematic representation of the flow field in the vicinity of a hard sphere moving close to a rigid wall. R_H is the hydrodynamic radius of the particle, h is the distance separating the particle from the wall and $\vec{v}_0$ (respectively, $\vec{v}_1$) is the velocity of the particle in the fluid (resp. at the wall surface)

not a rigorous consequence of the calculation, originally performed as an expansion in the *small* parameter R_H/d_w.

The drag force experienced by a particle owing to its motion parallel to the wall and at a distance h from it (Fig. 7) can be pictorially seen as resulting, in part, from the shear of the fluid layer separating the particle from the wall surface. With the help of this simple picture, it appears reasonable to expect that the shear becomes extremely large for $h \equiv -R_H + d_w/2$ going to 0. This divergence of the drag coefficient will, in turn, yields a diffusion coefficient $D_\perp$ going to 0 in this limit. This idea can be expressed by heuristically modifying eq. (4), adding a wall-induced drag to the conventional Stokes term as

$$\vec{F_0} = -6\pi\eta_0 R_H \left[\vec{v}_0 + \frac{R_H}{h}(\vec{v}_0 - \vec{v}_1)\right] \tag{7}$$

where $\vec{v}_1$ is equal to zero for rigid walls and R_H/h is a dimensionless parameter characterising the confinement. Using such a scheme, Faxén's lowest order expression for the diffusion coefficient $D_\perp$, eq. (6), is indeed recovered. This will prove useful in Section 4.4 below, when the picture of Fig. 7 is extended to the case of *fluid* walls, releasing the constraint $v_1 = 0$.

4.3 2D diffusion in a 3D space

A solid particle inserted into a liquid membrane freely diffuses in a space restricted to almost two dimensions, but coupled to the 3D solvent surrounding the membrane. Such a system was studied quantitatively by Saffman and Delbrück [21] and Hughes *et al.* [22]. A limiting expression for the diffusion coefficient reads:

$$D \approx \frac{k_B T}{4\pi} \frac{\ln\left(\frac{\eta_m \delta}{\eta_0 R_H}\right) - \gamma}{\eta_m \delta} \tag{8}$$

with $\gamma \approx 0.577$ the Euler constant, δ the thickness of the membrane, η_m the viscosity of the fluid membrane and η_0 the viscosity of the solvent on both sides of the membrane. For eq. (8) to be valid, $\eta_m\delta$ should be much larger than $\eta_0 R_H$ [22]. Obviously, it leads then to a diffusion coefficient in the membrane significantly smaller than would result from eq. (5) for the same particle embedded in the solvent.

It results from eq. (8) that the diffusion coefficient depends, for this particular two-dimensional problem, only logarithmically, that is to say weakly, on the particle size R_H. Note that this very property, investigated in numerous experimental studies [18, 49–51], has been recently contested, with a $1/R_H$ dependence shown to be sometimes more appropriate than the logarithmic relation, even in the small R_H limit [17, 19]. We shall nevertheless use eq. (8) in the present discussion, as it predicts a kind of "baseline" value for the diffusion coefficient D. In any case, the range here available for R_H variations is experimentally quite restricted.

4.4 Confined diffusion between fluid walls

The diffusion of a particle confined in a lamellar phase is a problem much more complex than those alluded to above. Altogether disregarding the role of elastic distortions in the lamellar stack–distortions altering not only the geometry of the water channels but also the distribution of the particles across them [52]–, we only consider here the effect of a finite bilayer viscosity: Contrarily to the case where walls are rigid, the velocity of the fluid dragged by the motion of the particle is no longer expected to fall to zero at the membrane surface. Then, in the simple picture of Fig. 7, $v_1 \neq 0$ but we shall not attempt to solve in any way the actual hydrodynamic problem. We simply consider, instead, that the particle immersed in the solvent channel, diffusing in a direction parallel to the membranes, will symmetrically drag part of the two surrounding bilayers. Furthermore, we consider the dragged part of the bilayer itself as a 2D-diffusing particle. In Section 4.3, the diffusion coefficient of the solid particle was not a strong function of the particle size. We therefore assume the 2D fluid particle twinned with the actual one to be also of size R_H.

In order to relate the yet unknown velocity $\vec{v}_1$ to the velocity $\vec{v}_0$ of the actual particle, we postulate an equality between the drag force acting on the bilayer-embedded particle and the wall-induced drag force acting on the actual particle, namely:

$$4\pi\eta_m\delta\beta(R_H)\vec{v}_1 = \frac{6\pi\eta_0 R_H^2}{h}(\vec{v}_0 - \vec{v}_1) \tag{9}$$

with $\beta(R_H) = \left[\ln\left(\frac{\eta_m\delta}{\eta_0 R_H}\right) - \gamma\right]^{-1}$ taken from the classical Saffman and Delbrück expression. The velocity of the bilayer-embedded particle, $\vec{v}_1$, can therefore be expressed as a function of the particle velocity:

$$\vec{v}_1 = \frac{\vec{v}_0}{1 + [2\alpha\delta\beta(R_H)h/(3R_H^2)]} \tag{10}$$

with α denoting the viscosity ratio η_m/η_0. The physical content of eqs. (9) and (10) appears to be satisfactory in both the large and small confinement limits: In the former case, there is little hydrodynamic coupling between the solvent and the fluid wall. The rigid wall situation where $v_1 = 0$ is recovered. In the latter case, the drag on the actual particle is dominated (for α large enough) by the drag on the bilayer-embedded particle.

Equation (7) may then be rewritten in a form now accounting for eq. (10), *i.e.* $v_1 \neq 0$:

$$\vec{F}_0 = -6\pi\eta_0 R_H \vec{v}_0 \left[1 + \frac{2\alpha\delta\beta(R_H)R_H}{3R_H^2 + 2\alpha\delta\beta(R_H)h}\right] \tag{11}$$

Eventually, the Einstein relation yields an expression for the diffusion coefficient of a particle symmetrically confined between two *liquid* walls:

$$D_\perp = D_0 / \left[1 + \frac{2\alpha\delta\beta(R_H)R_H}{3R_H^2 + 2\alpha\delta\beta(R_H)h}\right] \tag{12}$$

with D_0 the free-diffusion coefficient of the particle in the 3D solvent.

The above-described simple argument is designed for a Brownian particle diffusing in the *solvent* channel between the membranes and, therefore, cannot be applied "as is" when the width d_w of the solvent channel becomes less than the hydrodynamic diameter $2R_H$ of the particle, or $h \leq 0$. It should be noted, however, that the value of $D_\perp$ for h small (and positive) is, especially for a large viscosity ratio α, numerically close to the value for the diffusion coefficient of a particle actually inserted into the membrane, see eq. (8). This is, of course, not a fortuitous coincidence but a consequence of our self-consistent assumption, eq. (9), relative to the drag force acting on the membrane-embedded particle twinned with the actual particle when $h > 0$. As we have shown in Section 3 that there are experimental evidences for a still significant–though slow–Brownian dynamics in the concentrated regime, we tentatively propose to extend our description of the diffusion coefficient $D_\perp$ in the following way:

$$D_\perp = \begin{cases} D_\perp(h) & \text{if } h > 0 \\ D_\perp(h=0) & \text{if } h \leq 0 \end{cases} \tag{13}$$

where the function $D_\perp(h)$ is defined in eq. (12). Such a scheme amounts to saying that, when the thickness of the water layer becomes less than the particle size and whatever the actual particle location, the particle diffuses essentially like a hydrophobic probe located within an (isolated) membrane. For the ideal spherical shape chosen here, the transition between the two regimes happens for $2R_H/d_w = 1$, or $h = 0$.

For diffusing particles which are *not* spherical but, for instance, of an either prolate or oblate ellipsoidal shape, two parameters–the lengths of, respectively, the long $2R_>$ and short $2R_<$ axes, for instance–have to be introduced in order to characterise the particle geometry. In the case of moderately anisotropic particles, the hydrodynamic radius associated to the self-diffusion in a three-dimensional and *unconfined* medium is experimentally found to be numerically close to the value of the long-axis parameter, *i.e.* $R_H \approx R_>$. When such particles are confined in a lamellar phase, we expect their diffusive behaviour to be comparable to the one of spherical particles as long as their rotational motion remains unhindered, that is to say for d_w large enough compared to $2R_>$. In the case where d_w is smaller than $2R_>$, at least one among the three possible rotational degrees of freedom becomes plainly geometrically hindered, and the long axis of the particle has to lie essentially perpendicular to the optical axis. Such a situation is also expected to occur, even for d_w slightly greater than $2R_>$, when the confining walls are solid or fairly viscous because the oriented particles will then experience a reduced drag.

These considerations suggest that in eq. (8) and, therefore, in eq. (9) the dimensionless ratio R_H/h that expresses the coupling between the dragged solvent and the bilayers should be now replaced by $R_</(d_w/2 - R_<)$. In the intermediate situation, namely $d_w \gtrsim 2R_>$ and for *viscous* bilayers, though the rotational motion of the particle is not geometrically hindered yet, it seems quite permissible to consider configurations with the long axis of the particle *parallel* to the optical axis of the lamellar phase dynamically much less favourable, as far as Brownian motion perpendicular to the optical axis is concerned, than those appropriately rotated by 90 degrees. In order to estimate the drag enhancement due to confinement, the replacement of R_H/h by $R_</(d_w/2-R_<)$ (with thus $h \equiv d_w/2-R_>$) appears to be a reasonable hypothesis. A generalised form of eq. (12), to be used in eq. (13) with anisotropic particles and viscous bilayers, becomes then:

$$D_\perp = \frac{k_B T}{6\pi\eta_0 R_>}\left[1 + \frac{2\alpha\delta\beta(R_>)R_<}{3R_>R_< + 2\alpha\delta\beta(R_>)(d_w/2 - R_<)}\right]^{-1} \qquad (14)$$

4.5 Comparison with experiment

Figure 8 shows again the experimental data, already presented in Section 3, but we now plot $D_\perp/D_0$ as a function of the reduced variable $2R_H/d_w$, following the above-described analysis.

Note that D_0 and R_H correspond to the free (no confinement) Brownian motion of the respective particles in water and have been measured independently (see Table 1). Besides, the geometric parameters d_w and δ of the lamellar phases are known from x-ray measurements.

In order to compare the data with our analysis, a value for the viscosity ratio $\alpha \equiv \eta_m/\eta_0$ must be chosen. Our estimate of η_m proceeds as follows: With eq. (8) as a relation between the diffusion coefficient D, the hydrodynamic radius R_H and the bilayer viscosity, the latter is obtained from the measured D (see Table 1) when R_H is known. In the present case of DHPE-FITC embedded into surfactant membranes, we consider R_H to be equal to one half the square root of the area per (unlabelled) DHPE lipid in the *fluid* bilayer state at full hydration. Even though the DHPE–water system is known to be in the gel phase at room temperature [53], the alkyl chains are indeed unlikely to be in their ordered state when surrounded by a large amount of surfactant molecules. From the known increase of area per lipid across the gel-to-fluid transition of a rather similar lipid, namely the di-C_{16}-phosphatidylcholine lipid DPPC, we thus take $R_H \approx \sqrt{64}/2$ [54], or $R_H = 4$ Å as a reference value, which yields $\eta_m = 84$ mPa.s for the $C_{12}E_5$ system, and $\eta_m = 30$ mPa.s for AOT [1].

[1] Even though the *values* obtained for η_m may not be absolute ones, the use of eq. (8) is self-consistent since $\eta_m\delta \gg \eta_0 R_H$ is found in both cases

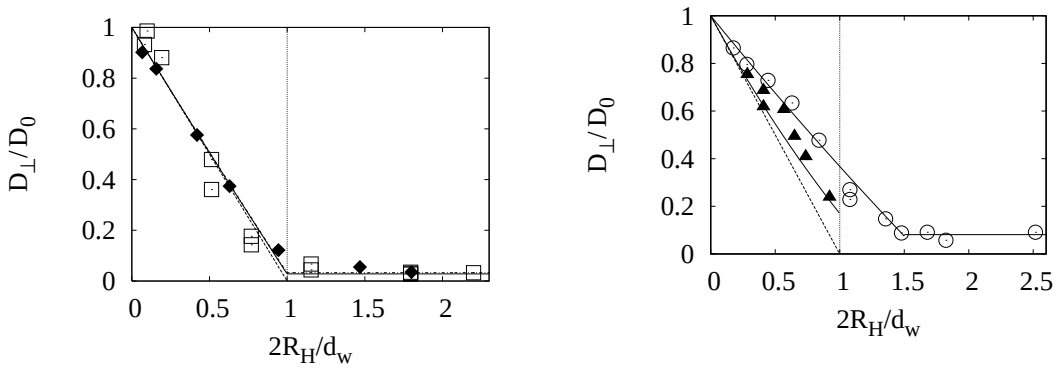

Figure 8: Same data as in Fig. 6, now plotted in the $(D_\perp/D_0)$ *versus* $(2R_H/d_w)$ representation. The vertical dotted line corresponds to $2R_H/d_w = 1$. The oblique dashed line corresponds to eq. (6). (a) Fluorescein (filled lozenges ⧫) or rhodamin (empty squares □) dyes inserted in the $C_{12}E_5$ / hexanol / water system. The solid (respectively, dash-dotted) line corresponds to eq. (13), without any adjustable parameters and R_H appropriate for fluorescein (resp. rhodamin). The transition between dilute and concentrated regimes happens for a water layer thickness (d_w) strictly equal to the hydrodynamic diameter of the particle: $2R_H/d_w = 1$ (b) Fluorescent protein (BSA*) inserted in the lamellar phase of the $C_{12}E_5$ / hexanol / water system (empty circle ∘) and of the AOT/NaCl/water system (full triangles ▲). The solid lines correspond to either eq. (13)–AOT system–or eq. (14)–$C_{12}E_5$ system, without any adjustable parameters

In Fig. 8a, the two (nearly superimposed) solid and dash-dotted lines correspond the predictions of eq. (12) with the appropriate values for the parameters δ, R_H and α. The fluid character of the bilayers has little influence on the drag coefficient and the simple model, eq. (6) or dashed line in Fig. 8, altogether neglecting fluidity, is quite satisfactory as long as $2R_H/d_w$ is less than 1. Though not very sensitive to α, the complete model is to be preferred, however, in that it predicts the cross-over from the dilute to the confined regime.

For BSA*, as noted previously, the confined regime is not observed with the AOT / NaCl / water system because the protein is expelled from the lamellar phase when $2R_H/d_w$ approaches 1. Describing the data in this restricted range with eq. (13), *i.e.* not considering the anisotropy of the protein to be relevant here owing to the low value of the membrane viscosity, appears successful, see Fig. 8b, and the deviation from the simple model, eq. (6), is rather conspicuous.

With BSA* inserted inside the $C_{12}E_5$ / hexanol / water lamellar phase, it is obvious from the representation chosen in Fig. 8 that the transition to the confined regime occurs *beyond* $2R_H/d_w = 1$. This result can be interpreted by taking into account the anisotropy of the protein, associated with a coupling between orientations and Brownian motion as expressed in eq. (14). Fig. 8b shows the prediction obtained using this latter model, once again without any adjustable parameters–the value for $R_<$, namely $R_< = 24$ Å or $R_H/R_< = 3/2$, being taken from small-angle neutron scattering data for BSA [55]. It is rewarding to observe that the proposed model accounts remarkably well for the experimental variation of the diffusion coefficient.

As final comments, one may wonder why the same protein, BSA*, is considered to be an isotropic particle when inserted in the AOT system, but as an anisotropic one in $C_{12}E_5$, and also why anisotropy is not considered for the other two dyes. In the latter case, the data is definitely not precise enough to capture meaningfully the anisotropy, if any, of the diffusing particles. With BSA* in AOT, we have tried the anisotropic description resulting from eq. (14)–*dynamically-oriented* proteins even at moderate confinement–, keeping the anisotropy ratio $R_H/R_<$ fixed to its known value. Only a poor description of the data is obtained. This probably means that

the bilayer viscosity is not high enough to induce a significant particle orientation, an orientation which cannot be reached geometrically either, since the protein is expelled from the lamellar phase at high confinement. Generally speaking, it is also worth remembering that many other important dynamical features of lamellar phases, primarily the layer displacement fluctuations, have been altogether left out of the heuristically-built considerations leading to eqs. (13) and (14). In this respect, a more detailed analysis, supported by more data, would be desirable.

5 Conclusions

We have measured in two distinct lamellar phases the in-plane self-diffusion coefficient $D_\perp$ of three fluorescent probes–two dyes, fluorescein and rhodamin; one fluorescently-labelled protein BSA*– as a function of the confinement d_w. All the probes display a first (dilute) regime with a quasi-linear relation between $D_\perp$ and $1/d_w$. This behaviour can be qualitatively, and even sometimes quantitatively, explained by Faxén's model for self-diffusion of a colloidal particle symmetrically confined between two rigid walls. We also observe a second (concentrated or confined) regime when the probes are inserted inside the $C_{12}E_5$ / hexanol / water lamellar phase. For the three probes, the self-diffusion coefficient does not go to zero but remains nearly constant for membrane separations d_w smaller than the particle size. In order to describe the existence of this confined regime, we develop simple heuristic arguments taking into account the fluidity of the membranes. The finite viscosity of the lipid bilayers is accounted for and modifies the diffusion properties of a hydrophilic probe moving parallel to the membranes. With this new model, we show the possible existence of a concentrated regime, *i.e.* for distances between membranes smaller than the size of the particles. We were able to establish experimentally that the limit between the two regimes is directly correlated to the diameter of the particle. For an anisotropic particle, like BSA*, our results suggest that the long axis of the ellipsoid is oriented parallel to the membranes. The transition between regimes appears at an intermembrane separation, corresponding to the smaller diameter of the ellipsoid ($R_<$). In favourable cases, similar experiments could thus testify the anisotropy of a probe inserted inside a lyotropic lamellar phase.

Acknowledgements

We gratefully acknowledge Professors L. Becus and M. Lenoblus for useless discussions.

References

[1] P. Tolédano, A.M. Figueiredo Neto, Phase transitions in complex fluids (River Edge, NJ: World Scientific, 1998)

[2] See, *e.g.*, Micelles, Membranes, Microemulsions and Monolayers, W.M. Gelbart, A. Ben-Shaul and D. Roux, Editors (Springer-Verlag, New York, 1994)

[3] P. Kékicheff, B. Cabane, M. Rawiso, *J. Colloid Interface Sci.*, **102**, 51 (1984)

[4] M. Singh, R. Ober, M. Kléman, *J. Phys. Chem.*, **97**, 11108 (1993)

[5] C. Ligoure, B. Bouglet, G. Porte, *Phys. Rev. Lett.*, **71**, 3600 (1993)

[6] E.Z. Radlinska, T. Gulik-Krzywicki, F. Lafuma, D. Langevin, W. Urbach, C.E. Williams, R. Ober, *Phys. Rev. Lett.*, **74**, 4237 (1997)

[7] M.-F. Ficheux, A.-M. Bellocq, F. Nallet, *J. Phys. II France*, **5**, 823 (1995)

[8] J. Kötz, S. Kosmella, *Curr. Opin. Colloid Interface Sci.*, **4**, 348 (1999)

[9] P. Fabre, C. Casagrande, M. Veyssié, V. Cabuil, R. Massart, *Phys. Rev. Lett.*, **64**, 539 (1990)

[10] V. Ponsinet, P. Fabre, *J. Phys. II France*, **6**, 955 (1996)

[11] P.L. Felgner, T.R. Gadek, M. Holm, R. Roman, H.W. Chan, M. Wenz, J.P. Northrop, G.M. Ringold, M. Danielsen, *Proc. Natl. Acad. Sci. USA*, **84**, 7413 (1987)

[12] J.O. Rädler, I. Kotlover, T. Salditt, C.R. Safinya, *Science*, **275**, 810 (1997)

[13] E.M. Landau, G. Rummel, S.W. Cowan-Jacob, J.P. Rosenbusch, *J. Phys. Chem. B*, **101**, 1935 (1997)

[14] M. Caffray, *Journal of Structural Biology*, **142**, 108 (2003)

[15] D.M. Anderson, H. Wennerström, *J. Phys. Chem.*, **94**, 8683 (1990)

[16] P. Fabre, C. Quilliet, M. Veyssié, F. Nallet, D. Roux, V. Cabuil, R. Massart, *Europhys. Lett.*, **20**, 229 (1992)

[17] Y. Gambin , R. Lopez-Esparza, M. Reffay, E. Sierecki, N. S. Gov, M. Genest, R. S. Hodges, W. Urbach, *Proc. Natl. Acad. Sci. USA*, **103**, 2098 (2006)

[18] P. Cicuta, S. L. Keller, S. L. Veatch, *J. Phys. Chem. B*, **111**, 3328 (2007)

[19] A. Naji, A. J. Levine, P. A. Pincus, *Biophys. J.*, **93**, L49 (2007)

[20] S. Kim, S.J. Karrila, Microhydrodynamics. Principles and selected applications (Mineola, NY: Dover Publications, Inc., 2005)

[21] P.G. Saffman, M. Delbrück, *Proc. Natl. Acad. Sci. USA* **72**, 3111 (1975)

[22] B. D. Hughes, B. A. Pailthorpe, L. R. White *J.Fluid Mech.* **110**, 349 (1981)

[23] A. Pralle, E.L. Florin, E.H.K. Stelzer, J.K.H. Horber, *Appl. Phys. A: Mater. Sci. Process.*, **66**, S71 (1998)

[24] Y.S. Ho, C.S. Johnson, Jr, *J. Chem. Phys.*, **74**, 2717 (1981)

[25] M. Jonströmer, R. Strey, *J. Phys. Chem.*, **96**, 5993 (1992)

[26] É. Freyssingeas, F. Nallet, D. Roux, *Langmuir*, **12**, 6028 (1996)

[27] W. Helfrich, *Z. Naturforsch. A*, **33**, 305 (1978)

[28] K. Fontell, *in* Colloid dispersion and micellar behavior; ACS Symposium Series 9, American Chemical Society, Washington DC (1975) 270

[29] M. Skouri, J. Marignan, R. May, *Colloid Polym. Sci.* **269**, 929 (1991)

[30] T.K.L. Meyris, S.C. De Smedt, P. Van Oostveldt, J. Demeester, *Pharm. Res.* **16**, 1153 (1999)

[31] D. Axelrod, D.E. Koppel, J. Schlessinger, E. Elson, W.W. Webb, *Biophys. J.* **16**, 1055 (1976)

[32] S. Seiffert, W. Oppermann, *Journal of Microscopy* **220**, 20 (2005)

[33] E.L. Gelamo, R. Itri, A. Alonso, J. Vasques da Silva, M. Tabak, *J. Colloid Interface Sci.* **277**, 471 (2004)

[34] P. Ganatos, S. Weinbaum, J. Pfeffer, *J. Fluid Mech.*, **99**, 739 (1980)

[35] P. Ganatos, R. Pfeffer, S. Weinbaum, *J. Fluid Mech.* **99**, 755 (1980)

[36] E. Gavze, M. Shapiro, *Int. J. Multiphase Flow* **23**, 155 (1997)

[37] H. Faxén, *Ann. Phys.* **68**, 89 (1922), quoted from J. Happel, B. Brenner, *in* Low Reynolds number hydrodynamics (Kluwer Academic Publishers Group, Dordrecht, 1983)

[38] S.H. Lee, R.S. Chadwick, L.G. Leal, *J. Fluid Mech.* **93**, 705 (1979)

[39] A. Einstein, *Ann. Phys. (N.Y.)* **17**, 549 (1905), quoted from A. Einstein, *in* Investigations on the theory of the Brownian movement (Dover, New York, 1956)

[40] L. P. Faucheux, A. J. Libchaber, *Phys. Rev. E*, **49** (1994) 5158

[41] D.G. Grier, *Curr. Opin. Colloid Interface Sci.* **2**, 264 (1997)

[42] B. Lin, J. Yu, S. A. Rice, *Phys. Rev. E* **62**, 3909 (2000)

[43] E. R. Dufresne, D. Altman, D.G. Grier, *Europhys. Lett.* **53**, 264 (2001)

[44] L. Lobry, N. Ostrowsky, *Phys. Rev. B* **53**, 12050 (1996)

[45] F. Nadal, A. Dazzi, F. Argoul, B. Pouligny, *Appl. Phys. Lett.* **79**, 3887 (2001)

[46] P. Lançon, G. Batroumi, L. Lobry, N. Ostrowsky, *Physica A* **304**, 65 (2002)

[47] B. Cui, H. Diamant, B. Lin, S. A. Rice, *Phys. Rev. Lett.* 92, 258301 (2004)

[48] Y. Han, A.M. Alsayed, M. Nobili, J. Zhang, T.C. Lubensky, A.G. Yogh, *Science* **314**, 626 (2006)

[49] E. A. J. Reits, J. J. Neefjes, *Nat. Cell Biol.* **3**, 145 (2001)

[50] N. Kahya, E.-I. Pecheur, W. P. de Boeij, D. A. Wiersam, D. Hoekstra *Biophys. J.* **81**, 1464 (2001)

[51] N. Tsapis, F. Reiss-Husson, R. Ober, M. Genest, R. S. Hodges, W. Urbach *Biophys. J.* **81**, 1613 (2001)

[52] T. Bickel, M. Benhamou, H. Kaïdi *Phys. Rev. E* **70**, 051401 (2004)

[53] B. Tenchov, R. Koynova, M. Rappolt, G. Rapp, *Biochim. Biophys. Acta*, **1417**, 183 (1999)

[54] J.F. Nagle, S. Tristram-Nagle, *Biochim. Biophys. Acta*, **1469**, 159 (2000)

[55] A. Das, R. Chitra, R.R. Choudhury, M. Ramanadham, *Pramana - J. Phys.* **63**, 363 (2004)